hiPSC-derived 3D cardiac microtissue models with integrated immune cells and vasculature

Arslan-van Bergen, U.

Development of Vascularized hiPSC-derived 3D cardiac microtissue on chip

Authors and Affiliations

Ulgu Arslan[1], Marcella Brescia[1], Viviana Meraviglia[1], Dennis M. Nahon[1], Ruben W.J. van Helden[1], Jeroen M. Stein[1], Francijna E. van den Hil[1], Berend J. van Meer[1], Marc Vila Cuenca1[1,2], Christine L. Mummery[1], Valeria V. Orlova[1]*

[1]Department of Anatomy and Embryology, Leiden University Medical Centre, 2333ZC Leiden, The Netherlands

[2]Department of Clinical Genetics, Leiden University Medical Center, 2333ZA Leiden, the Netherlands

* Corresponding author

This work was combined with the study in chapter 6 and published in Stem Cell Reports, 2023 Jul 11, 18:1394–1404.
DOI: 10.1016/j.stemcr.2023.06.001.

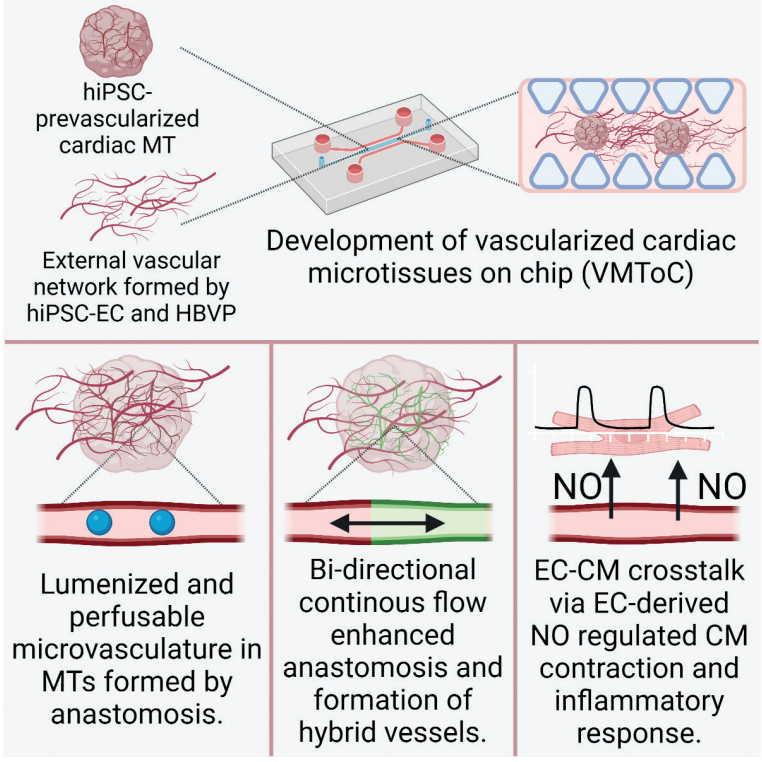

Graphical abstract

Summary

Functional vasculature is essential for delivering nutrients, oxygen and cells to the heart and removing waste products. Here, we developed an *in vitro* vascularized human cardiac microtissue (MT) model based on human induced pluripotent stem cells (hiPSCs) in a microfluidic organ-on-chip by co-culturing hiPSC-derived, pre-vascularized, cardiac MTs with vascular cells within a fibrin hydrogel. We showed that vascular networks spontaneously formed in- and around these MTs and were lumenized and interconnected through anastomosis. Anastomosis was fluid flow-dependent: continuous perfusion increased vessel density and thus enhanced the formation of the hybrid vessels. The model establishes the groundwork to integrate perfusable vasculature in microtissue/organoids, enabling the study of cellular crosstalk and its effect on functionality.

Keywords:

human induced pluripotent stem cells; cardiac microtissue; heart-on-chip.

Introduction

Cardiovascular disorders are a major cause of death around the world. The heart is a highly metabolic organ and has high energy demands for proper function. Endothelium is crucial in this process as it forms a semi-permeable barrier between cardiomyocytes (CM) and the blood, providing selective nutrient, oxygen and drug delivery to heart cells. It also mediates immune cell trafficking, for example, in the case of inflammation (Amersfoort et al., 2022). Interruption of the blood supply can lead to CM death, as in myocardial infarction (Berry and Duncker, 2020), and successful heart transplantation requires rapid restoration of blood supply to the donor heart.

Some of the current 3D microphysiological models (reviewed in Arslan et al., 2022) incorporated vascular networks inside engineered tissues but in general they were not perfusable by fluid or blood (equivalents) (Zhang et al., 2021). This has in part been addressed by either integrating organoids into a microfluidic chip or implanting them into living animals, as perfusion is also necessary for the stability and integrity of the microvascular networks (Mansour et al., 2018; Ryan et al., 2021; Takebe et al., 2013).

In the study here, we developed a fully vascularized and perfusable cardiac microtissue (MT) on-chip by integrating pre-vascularized cardiac MTs with an external vascular network formed by self- organization of human induced pluripotent stem cell derived endothelial cells (hiPSC-ECs) and human brain vascular pericytes (HBVPs) in fibrin hydrogel in a microfluidic organ-on-chip. The integration of MTs in the chips did not adversely affect formation of the external, self-organized vascular network and these networks developed robustly, inside- and around the MTs. Using this model, we demonstrated that cardiac MTs can be efficiently vascularized within days and the lumenized vascular networks in-

Figure 1

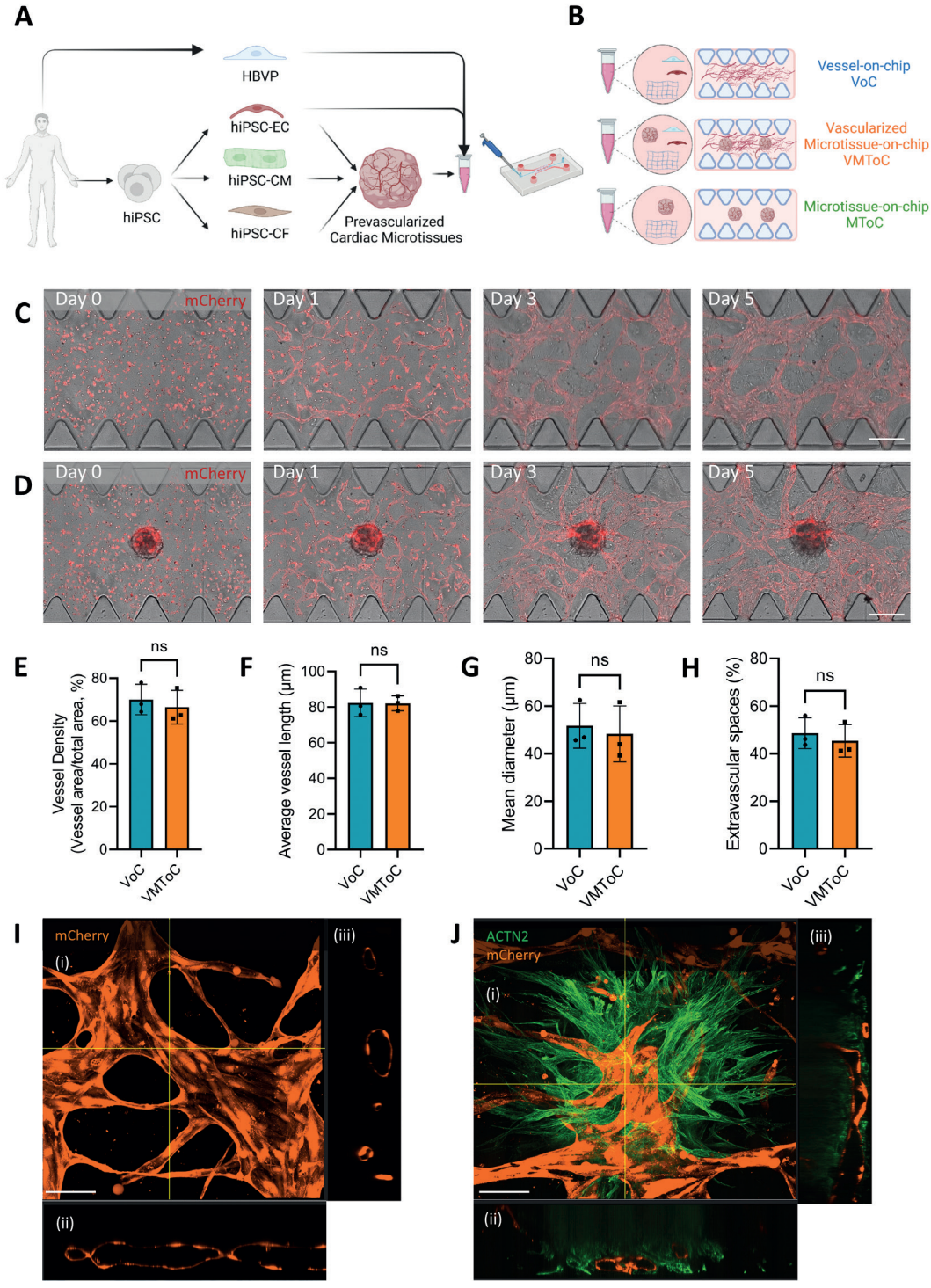

Figure 1: Characterization of the vascular network in the presence of cardiac MTs. *(A, B) Schematic overview of the vascularized cardiac MTs experimental setup (A) and conditions used in the study (B). hiPSC-EC and HBVPs*

were cocultured to form VoC; hiPSC-MTs were cocultured with hiPSC-EC and HBVPs to form VMToC; hiPSC-MTs were integrated into chips without any additional vascular cells to form MToC. (C, D) Representative images from chips on day 0, 1, 3 and 5 after seeding in the chips, which shows the development of external vascular networks in VoC (C), and VMToC (D). Images showing brightfield and hiPSC-EC (red, mCherry) (10×). Scale bars, 300 µm. (E-H) Quantification of vessel density (%) (E), average vessel length (µm) (F), mean diameter (µm) (G), extravascular spaces (%) (H). Error bars are shown as mean±SD from N = 3; three independent experiments with at least six microfluidic channels per experiment. Student's t-test; ns, not significant. (I, J) Representative confocal images of microvascular network in VoC (I) and VMToC (J) showing hiPSC-ECs (orange, mCherry) and hiPSC-CM (green, ACTN2). Images displaying maximum projection in xyz (i), xy (ii), and yz cross-sectional perspectives (iii) (40×). Scale bar, 100 µm. See also Video S1-3.

and around the MTs can be perfused. This may ultimately allow selective nutrient or drug delivery to the cells via the endothelial barrier inside the MTs, mimicking heart tissue *in vivo* even more closely.

Results

Characterization of the vascular network in the presence of cardiac MTs

The VMToC model was generated by combining prevascularized cardiac MTs (Giacomelli et al, 2020; Campostrini et al, 2021) with hiPSC-ECs and HBVPs, in a fibrin hydrogel. This MT/cell/hydrogel mix was then embedded in the gel channel of commercially available AIM Biotech 3D cell culture chips (Figure 1A). To investigate the effect of cardiac MTs on vascular network formation, we compared the VMToC model with a standard vessel-on-chip (VoC) that included hiPSC-EC and HBVP cocultures but without cardiac MTs (Figure 1B). Vascular organization in VoCs and VMToCs was already evident on day 1 (Figure 1C and D). On day 3, a complex vascular network had formed in the chips and these networks were stabilized by day 5. Quantification of the vascular network parameters such as vessel density (Figure 1E), average vessel length (Figure 1F), mean vessel diameter (Figure 1G) and extravascular space (Figure 1H) showed no significant differences between VoC and VMToC conditions. Vascular networks in VoC (Figure 1I) and the microvasculature in MTs in VMToC (Figure 1J, Video S1) were both lumenized.

To investigate whether the lumenized vasculature in cardiac MTs was actually perfusable, fluorescent beads (2 µm) were introduced into the medium in one of the media inlets of the chips. Beads entered the vascular networks from the intersection of medium-gel channel and moved spontaneously to the microvasculature in MTs (Figure 2A). Beads stayed within the microvasculature contours in the MTs indicating the interconnected vessels in the MTs were indeed perfusable (Figure 2B-E, Video S2 and S3).

Mechanism of the intra-microvascular network formation

In order to investigate the mechanism of the intra-microvascular network formation, we used hiPSC- ECs derived from two different fluorescent reporter lines (expressing mCherry or GFP). GFP- expressing hiPSC-ECs were used to prevascularize the cardiac

Figure 2

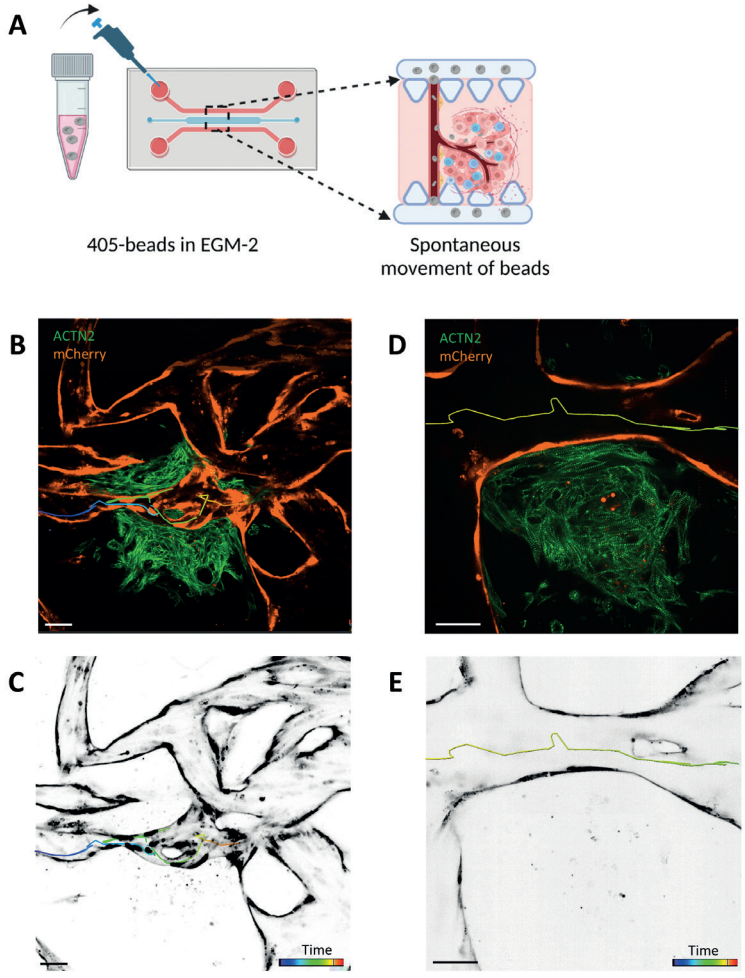

Figure 2: Cardiac MTs induce pulsative intra-microvascular flow. *(A) Schematic of the fluorescent beads (2 μm) perfusion experiment. Please see Supplemental Experimental Setup for experimental details. (B, D) Representative confocal images showing hiPSC- ECs (orange, mCherry) hiPSC-CM (green, ACTN2) and perfusion of 2 μm fluorescent beads (traces) in VMToC. (B is 20x and D is 40x with Scale bar, 50 μm. (C, E) Representative confocal images in black and white showing only vascular networks (black) and traces of beads inside (colored traces). Color coded bars represent time. Images are duplications of B and D. Scale bar, 50 μm.*

MTs and these MTs were cocultured with mCherry-expressing hiPSC-ECs and HBVPs in the chips (Figure 3A). Internal microvasculature in the MTs and external vascular network around MTs underwent anastomosis as early as day 2. Anastomosis was bidirectional in the system: (i) outside-in anastomosis where the external network invaded the MTs and anastomosed with the internal microvasculature in the MTs (Figure 3B and D); (ii) inside-out anastomosis where part of the internal microvascular network migrated outside the MT and anastomosed with the external vascular network (Figure 3C and E). As a result, hybrid vessels composed of hiPSC-ECs partly from MTs and partly from external vascular networks

Figure 3

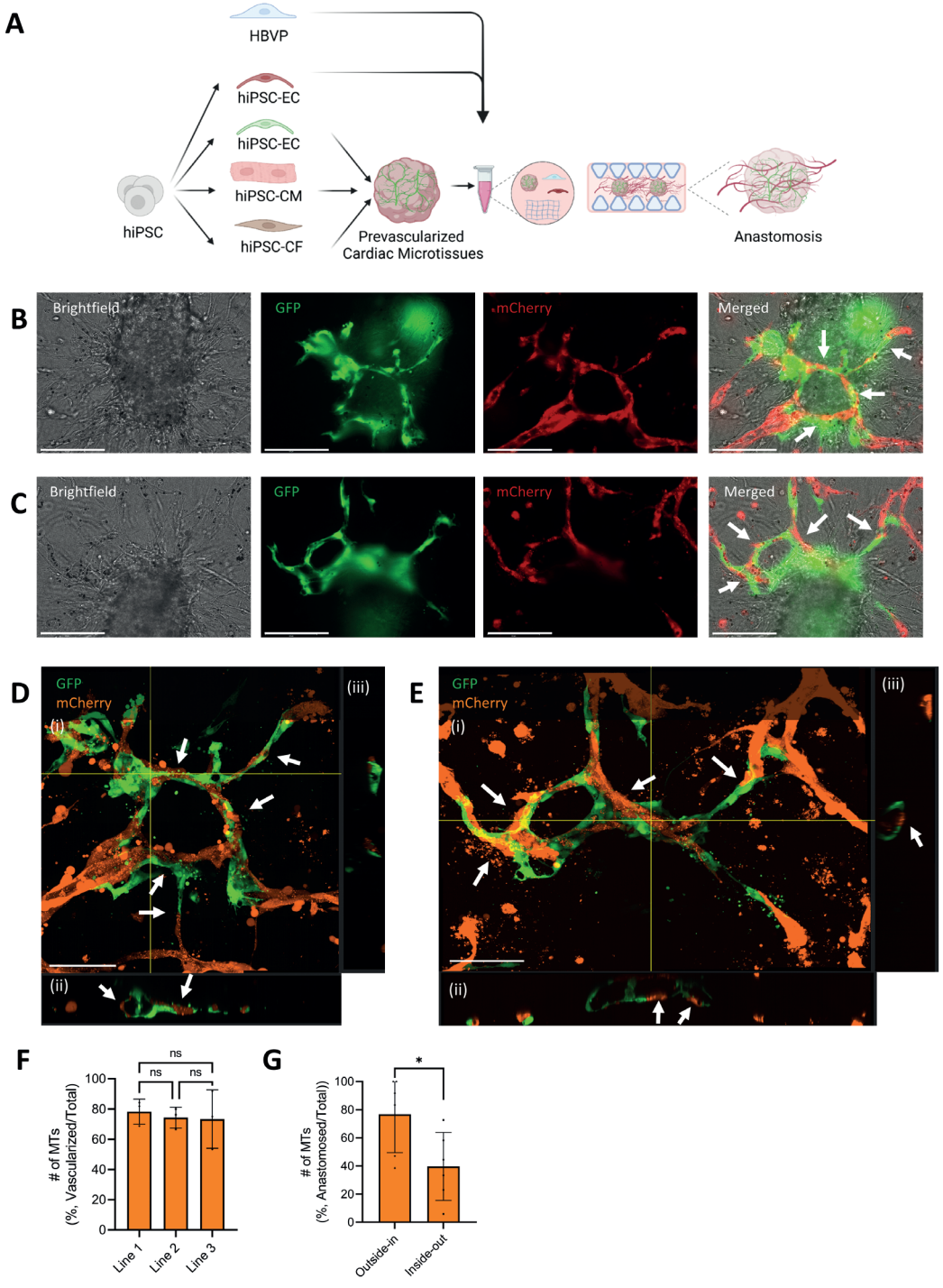

Figure 3: Mechanism of the intra-microvascular network formation. *(A) Schematic of the experimental setup. MTs were generated combining hiPSC-CMs, hiPSC-ECs (green, GFP) and hiPSC-CFs. These MTs were cocultured*

*with hiPSC-ECs (red, mCherry) and HBVPs in chips. (B, C) Representative images of outside-in (B) and inside-out (C) anastomosis and formation of hybrid vessels by interconnection of internal microvascular network (green, GFP) and external vascular network (red, mCherry) (20x). Scale bar, 150 μm. (D, E) Representative confocal images of hybrid vessels visible in B and C, respectively. Internal hiPSC-EC (green, GFP), external hiPSC-ECs (orange, mCherry). Images displaying maximum projection in xyz (i), xy (ii), and yz cross-sectional perspectives (iii) (40×). Scale bar, 100 μm. Arrows indicating the anastomosed points and hybrid lumens. (F) Quantification of number of vascularized MTs (%, number vascularized MTs/Total number of MTs). MTs contained CMs from three different hiPSC lines. Error bars are shown as mean±SD from N=3; three independent experiments with at least 10 MTs in each experiment. One- way ANOVA, ns, not significant. (G) Quantification of number of anastomosed MTs (%, #Anastomosed MTs/Total # of MTs) in independent experiments. Error bars are shown as mean±SD from N=6; six independent experiments with at least 9 MTs in each experiment. Student's t-test, *p < 0.05.*

were formed. Confocal images showed that these hybrid vessels were lumenized (Figure 3D and E). The number of vascularized tissues was comparable in all independent experiments (Figure 3F), with higher numbers of MTs showing evidence of outside-in anastomosis than those showing inside-out anastomosis (Figure 3G).

Since fluid flow is known to promote EC migration, proliferation and survival (Abe et al., 2019; Galie et al., 2014; Zhang et al., 2022) , we tested whether we could enhance the vascularization of cardiac MTs by introducing perfusion using a rocker (Figure 4A). Both intermittent and continuous perfusion resulted in anastomosis between the internal microvasculature and external vascular networks (Figure 4B and C, respectively).

However, continuous perfusion resulted in higher mCherry+ and GFP+ vessel density (Figure 4D-E) in the chips. Intermittent perfusion resulted in the formation of hybrid vessels where only a minority of cells originated in the cardiac MTs (Figure 4F). This improved substantially under continuous perfusion (Figure 4G).

Discussion

In the present study, we established vascularized and perfusable cardiac MT on a microfluidic organ- on-chip platform (VMToC) with vascular cells self-organised in fibrin hydrogel. The external vascular cells reproducibly formed a continuous vascular network in- and around the MTs and this was not affected by contraction of the MTs. Continuous perfusion generated by placing the chips on a rocker resulted in greater vascularization, improved anastomosis and enhanced formation of hybrid vessels. Since mechanistic studies on molecular pathways mediating anastomosis are challenging *in vivo*, this platform could provide an alternative way to understand this process *in vitro*. Furthermore, these networks developed robust lumens that contracted rhythmically in synchrony with surrounding CMs. This rhythmic contraction of CMs resulted in the generation of bidirectional flow as indicated by oscillatory movement of fluorescent beads into- and through the organized vascular network inside of the MT. Currently, no animal models are available that model ischemic heart disease caused by coronary microvascular obstruction (Niccoli et al., 2016; Sorop et al., 2020). Therefore, vascularized and perfusable cardiac MTs could be useful in

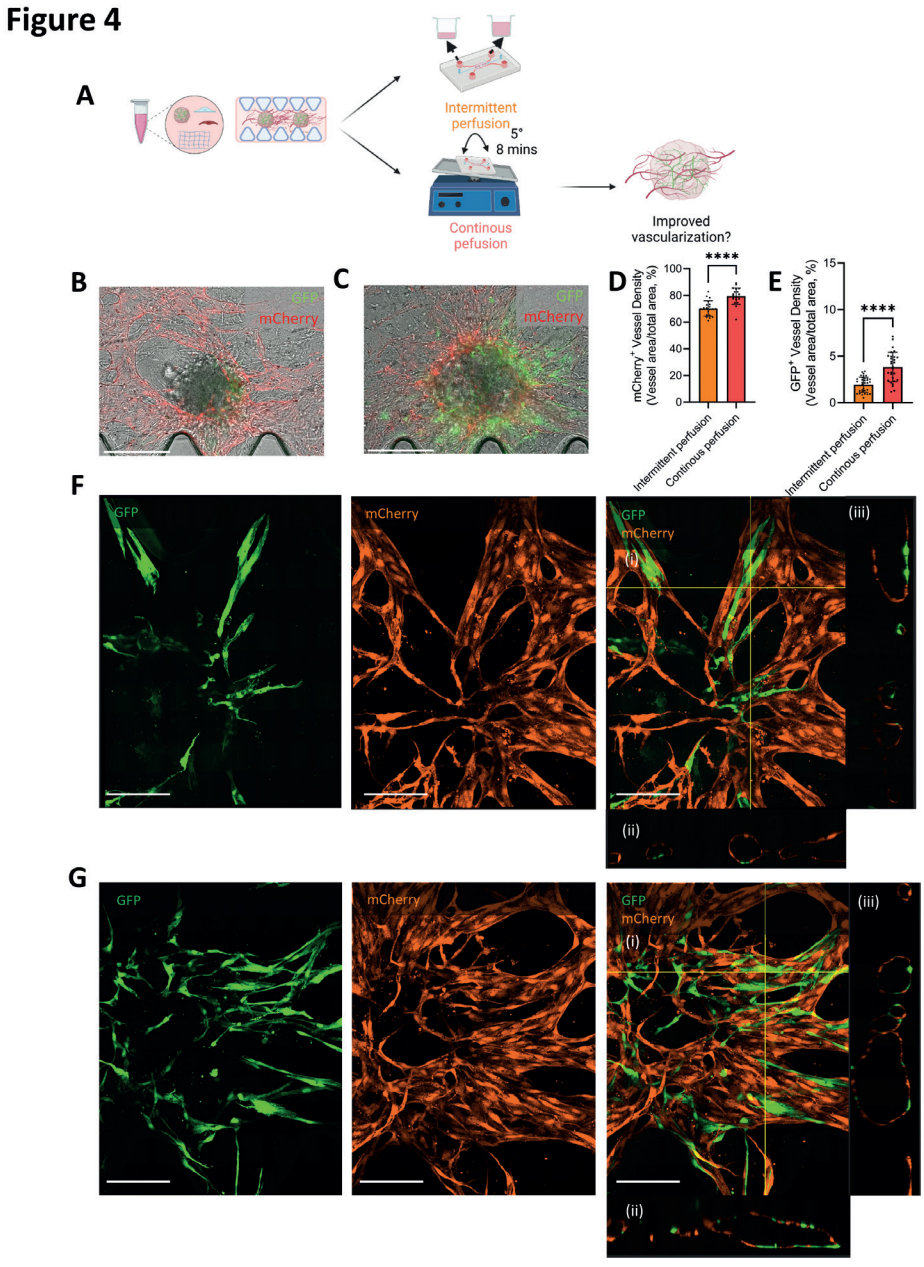

Figure 4: Continuous perfusion enhances vascularization of cardiac MTs. *(A) Schematic of the experimental setup for intermittent and continuous perfusion conditions. Chips were kept under intermittent gravity-driven flow with the medium exchange every 24 h or placed on the rocker (at a 5 degrees inclination angle and 8 min interval) to induce continuous perfusion through passive leveling between the reservoirs. (B, C) Representative images of VMToC under intermittent perfusion (B) and continuous perfusion (C) where anastomosis is visible by the formation of hybrid vessels (10x). Scale bar, 300 μm. (D) Quantification of mCherry+ vessel density (%) in intermittent and continuous perfusion conditions. Error bars are shown as ±SD from N = 3, n = 19 (intermittent perfusion) and n = 20 (continuous perfusion); three independent experiments with at least six microfluidic channels*

*per experiment. (E) Quantification of GFP+ vessel density (%) in intermittent and continuous perfusion conditions. Error bars are shown as ±SD from N = 3, n = 35 (intermittent perfusion) and n = 29 (continuous perfusion); three independent experiments with at least six microfluidic channels per experiment. (F, G) Representative confocal images of hybrid vessels formed in intermittent perfusion (F) or continues perfusion (G) conditions. Internal hiPSC-EC (green, GFP), external hiPSC-EC (orange, mCherry). Images displaying xyz (i), xy (ii), and yz cross-sectional perspectives (iii) (40×). Scale bar, 150 μm. Wilcoxon-Mann-Whitney test (D, E), ****p < 0.0001.*

studying mechanisms underlying microvascular obstruction using cardiac and vascular cells derived from patients.

Finally, although the formation of the vascular networks was robust in VMToC, we observed some batch-to-batch and plate-to-plate variability in the degree of vascularization. Vascularization of MTs was mostly through the anastomosis, so the extent of pre-vascularization in MTs might contribute to variability. In some cases where MTs were not well-vascularized, vascularization was improved by introducing continuous perfusion during later stages of culture (data not shown).

In summary, we demonstrated that 3D cardiac MTs can be integrated into microfluidic chips with the external vascular network formed by hiPSC-ECs and HBVPs. Using this model, we demonstrated that cardiac MTs can be efficiently vascularized within days and the lumenized vascular networks in- and around the MTs can be perfused. This may ultimately allow selective nutrient or drug delivery to the cells via the endothelial barrier inside the MTs, mimicking heart tissue *in vivo* even more closely. Our vascularized cardiac MT model thus provides a foundation for studies on organ-specific cellular communication, specifically for the endothelial barrier, drug screening and disease modelling.

Experimental Procedures

hiPSC lines and maintenance

hiPSCs were maintained on recombinant vitronectin-coated plates in TeSR-E8, all from STEMCELL Technologies, according to the manufacturer's instructions. The following hiPSC lines were used in this study: LUMC0059iCTRL03 (generated from skin fibroblasts, https://hpscreg.eu/cell-line/LUMCi026-A), LUMC0020iCTRL06 (generated from skin fibroblasts, https://hpscreg.eu/cell- line/LUMCi028-A) (Zhang et al., 2014); NIH Center for Regenerative Medicine: NCRM-1 (generated from CD34+ cord blood cells, https://hpscreg.eu/cell-line/CRMi003- A), obtained from RUDCR Infinite Biologics at Rutgers University, was modified in-house with a mCherry or GFP expression cassette under the human cytomegalovirus (hCMV) early enhancer/chicken β actin (CAG) promoter using a previously established protocol (Rostovskaya et al., 2012); The Allen Cell Collection: AICS-0075 (generated from skin fibroblasts, https://hpscreg.eu/cell-line/UCSFi001-A-4) with mEGFP insertion site at ACTN2 was obtained from Coriell Institute for Medical Research. hiPSC lines and cell batches of hiPSC-CMs, hiPSC-ECs and hiPSC-CFs are listed in Table 1.

Differentiation of cardiomyocytes

CM differentiation of hiPSC was induced in monolayer as described previously (Berg et al., 2016; Giacomelli et al., 2017). Briefly, 25 × 103 cells per cm2 were seeded on plates coated with 75 µg/ml growth factor-reduced Matrigel (Corning) the day before the start of differentiation (day -1). On day 0, cardiac mesoderm was induced by changing E8 to B(P)EL medium (Bovine Serum Albumin [BSA] and Essential Lipids), supplemented with a cytokine mixture (20 ng/ml BMP4, R&D Systems; 20 ng/ml ACTIVIN A, Miltenyi Biotec; 1.5 µM GSK3 inhibitor CHIR99021, Axon Medchem). After 3 days, cytokines were removed and XAV939 which is WNT inhibitor (5 µM, Tocris) was added for 3 days. After this, B(P)EL medium was refreshed every 3 days.

Differentiation of cardiac fibroblasts

CFs were differentiated from hiPSC using an epicardial (EPI) monolayer differentiation protocol (Guadix et al., 2017) as a starting point (Giacomelli et al., 2020). Briefly, 25 × 103 cells per cm2 were seeded on Matrigel at day -1. On day 0, cardiac mesoderm was induced as described above. After 3 days, cytokines were removed and XAV939 (5 µM) was added for 3 days with BMP4 (30 ng/ml) and Retinoic Acid (RA; 1 µM; Sigma Aldrich). On day 6, B(P)EL medium supplemented with BMP4 (30 ng/ml) and RA (1 µM) was refreshed. On day 9, 15 × 103 per cm2 were seeded on plates coated with 5 µg/ml of fibronectin from bovine plasma (fibronectin; Sigma Aldrich) in B(P)EL medium supplemented with the TGFβ inhibitor SB431542 (10 µM; Tocris). By day 12, EPIs were confluent and ready for passaging or analysis. EPI cells (30 cm2 per vial) were cryopreserved in CryoStor CS10 medium (0.5 ml/vial; Stem Cell Technologies).

CF differentiation was induced in monolayer. Briefly, 25 × 103 EPIs were seeded per cm2 on tissue culture plates coated with vitronectin in B(P)EL medium supplemented with FGF2 (10 ng/ml; R&D Systems) on day 12. On day 13 and every 2 days thereafter, medium was refreshed with B(P)EL supplemented with FGF2 (10 ng/ml). After 6 days (on day 19), CFs were expanded by changing B(P)EL to Fibroblast Growth Medium 3 (FGM3; PromoCell). FGM3 was refreshed every 2 days for approximately 10 days in total. After 10 days (on day 29), CFs were confluent and ready to be passaged at 1:2 ratio. FGM3 was refreshed the day after passaging and every 2 days thereafter. CFs (10cm2 per vial) were cryopreserved in CryoStor CS10 medium (0.5 ml/vial; Stem Cell Technologies).

Differentiation of endothelial cells

hiPSC differentiation to ECs was performed as described previously (Orlova et al., 2014). Briefly, hiPSCs were maintained in mTeSR-E8 medium. For mesoderm induction (day 0-3), mTeSR-E8 medium was replaced with B(P)EL medium supplemented with 8 µM CHIR99021 (Tocris Bioscience, 4423). Cells were refreshed with vascular specification medium comprised of VEGF (50 ng/ml) and 10 µM SB431542 (Tocris Bioscience, 1614) in B(P)EL at day

3, day 6, and day 9. hiPSC-ECs were isolated on day 10 using CD31-DynabeadsTM (Thermo Fisher Scientific), as previously described (Orlova et al., 2014). hiPSC-ECs were expanded in complete EC growth medium (EC-CGM) comprised of Human Endothelial-serum free medium (EC-SFM) with 1% Human platelet poor serum (P2918, Sigma), VEGF (30 ng/ml) and bFGF (20 ng/ml), as described previously with minor modifications (Orlova et al., 2014). hiPSC-ECs were expanded for additional 3-4 days post-isolation and cryopreserved using cryopreservation medium consists of 50% fetal bovine serum,40% EGM2 and 10% dimethyl sulfoxide at passage number 1 (P1) (StemCell Technologies, 07930).

3D cardiac microtissue formation

MTs were formed as described previously (Giacomelli et al., 2020). Prior to MT formation, hiPSC-ECs and hiPSC-CFs were prepared as follows: 3-4 days before MT formation, a vial of cryopreserved hiPSC-ECs and a vial of cryopreserved hiPSC-CFs were thawed and cultured either in EC-CGM on plates coated with gelatin (hiPSC-ECs), or in FGM3 on uncoated plates (hiPSC-CFs). On the day of MT formation (day 0), hiPSC-ECs and hiPSC-CFs were detached using TrypLE 1X for 2-3 mins at RT (EC) and 5 mins at 37 °C, 5 % CO2 (CF), centrifuged for 3 min at 1100 rpm, resuspended in B(P)EL medium and counted. hiPSC-CMs at day 14-21 that showed > 80 % purity, measured as the percentage of troponin positive cells by FACS, were dissociated using the TryplE 5X for 10 mins at 37 °C, 5 % CO2, resuspended in B(P)EL medium and counted. Cell suspensions were combined to a total of 5000 cells (70 % CM, 15 % EC and 15 % CF) per 50 µl B(P)EL medium supplemented with VEGF (50 ng/ml) and FGF2 (5 ng/ml). For all MTs, cell suspensions were seeded on V-bottomed 96-well microplates (Greiner bio-one) and centrifuged for 10 min at 1100 rpm. MTs were incubated at 37 °C, 5 % CO2 for 12 days with media refreshed every 3-4 days.

Cell Preparation before on chip culture

Human brain vascular pericytes (HBVPs) were purchased from ScienceCell. HBVPs were cultured in Pericyte Medium (ScienceCell, 1201) supplemented with Pericyte Growth Supplement (ScienceCell, 1252) and 2 % FBS. Cells were cryopreserved at passage number 3 (P3) using serum-free cryopreservation medium (CryoStorTMCS10) (StemCell Technologies, 07930). hiPSC-ECs (P1) were thawed and cultured on gelatin-coated plates in EC-CGM, 4 days prior to VoC seeding. HBVPs (P3) were thawed and cultured in Pericyte Medium (ScienceCell, 1201) supplemented with Pericyte Growth Supplement (ScienceCell, 1252) and 2 % FBS.

Microfluidic chip culture

Cell preparation prior to chip seeding was described in supplemental information. Commercially available microfluidic chips (AIM Biotech) were used. Cell and MT mixtures were prepared as follows: 1) 4 MT/channel in combination with 25 × 106 hiPSC-ECs/mL and 5 × 106 HBVP cells/mL (5:1 ratio) (VMToC); or 2) 25 × 106 hiPSC-ECs/mL and 5

× 106 HBVP cells/mL (VoC) were resuspended in endothelial growth medium-2 (EGM-2, Lonza) supplemented with Thrombin (4 U/mL) and then gently mixed with fibrinogen (final concentration 3 mg/mL, Sigma) at 1:1 vol ratio. Cell/hydrogel mixture was quickly loaded into the middle gel-loading channel of the microfluidic chip. Chips were incubated at room temperature for 15 min. To support vascular network formation in the presence of cardiac MTs we used a mixture of CM and EC growth medium (bovine serum albumin (BSA) and essential lipids (B(P)EL) medium and endothelial growth medium-2 (EGM-2); 50:50), supplemented with vascular endothelial growth factor (VEGF) (50 ng/mL). The γ-secretase inhibitor DAPT (10 µM) was also added to the medium on day 1 for 24 h. Intermittent gravity-driven flow in the whole chamber was induced by creating hydrostatic pressure through the addition of 100 µL medium to the right media ports and 50 µL media to left media ports in the medium channel. Medium was refreshed daily. For the continuous perfusion experiments microfluidic chips were placed on the interval rocker platform (Perfusion rocker, MIMETAS) set at a 5 degrees inclination angle and an 8 min interval from day 0 onwards. Chips were maintained until day 7 and characterized between day 5-7.

Imaging of vascularized 3D cardiac microtissues on chip

Whole channel images were captured daily with EVOSM7000 using 10x objectives. For automated imaging of whole channels and stitching, a customized plate layout was used. VMToCs and MToCs were fixed for 30 mins at 4 °C with 4% paraformaldehyde, washed 3 times in PBS (Calcium, Magnesium) and stored at 4 °C until processing. Confocal images were captured to create 3D stack using Andor Dragonfly spinning disk confocal microscope using a 20x or 40x objective. Image processing was done using Imaris 9.5 software (Bitplane, Oxford Instruments).

Characterization of vascular networks

Fields of views (FOV) from the full channels (acquired using EVOS) were arranged in size of 480X1200 pixels around the MTs. For VoC 75 FOVs and for VMToC 87 FOVs were captured from three independent experiments with at least six microfluidic channels each. These FOVs (Figure 1E-H), whole microfluidic channels (Figure S2D), and 10x images of MTs from channels (Figure S2E) were then quantified using pipelines developed on the free open source CellProfiler software (https://cellprofiler.org/) (Carpenter et al., 2006; Vila Cuenca et al., 2021). Briefly, for vessel density, pre-processing steps were applied to all images to enhance image features and a gaussian filter to reduce unspecific object identification. Two filter steps were applied to images of vascular network to reduce non-specific segmentation from cell junctions and a minimum cross-entropy thresholding method was used to produce a binarized image. The binarized images from the CellProfiler output were then analyzed using the freely available ImageJ software with a plugin

(https://imagej.nih.gov/ij/ ,https://imagej.net/DiameterJ) (Hotaling et al., 2015).

Fluorescent beads perfusion assay

Perfusion assessment of VMToC was done as described previously (Vila Cuenca et al., 2021). In brief, 405-beads (1 drop in 10 or 20 ml EGM-2, Fluoro-Max Dyed Blue Aqueous Fluorescent Particles, B0200, ThermoFisher Scientific) were added to the right medium port (100 µl) and to all other media ports (50 µl). Then, confocal image stacks and videos of the spontaneous move of the beads following the endothelial networks were acquired using DragonFly spinning disk (Andor) microscope with 20x and 40x magnification objective. Tracking of the beads was done using 3D rendering and cell tracking function in Imaris 9.5 software (Bitplane, Oxford Instruments).

Statistical analysis

Statistical analysis was performed using GraphPad Prism 9. Student's t-test, one-way ANOVA for paired or unpaired measurements were applied as appropriate to test for differences in means between groups/conditions. Kruskal–Wallis test and Wilcoxon-Mann-Whitney test were used when the normality assumption did not hold. Data are expressed and plotted as the Mean ± SD. as indicated in figure legend. Detailed statistics and exact P-values are indicated in each figure legend. Statistical significance was defined as $P < 0.05$.

Acknowledgements

We acknowledge LUMC confocal imaging facility for help with imaging and the Allen Cell Collection, available from Coriell Institute for Medical Research, for providing materials. We thank Mervyn Mol for help with CM differentiation. Images were generated using Biorender.com.

This work was supported by the European Union's Horizon 2020 research and innovation programme under grant agreement No. 812954; the Netherlands Organ-on-Chip Initiative which is an NWO Gravitation project (024.003.001) funded by the Ministry of Education, Culture and Science of the government of the Netherlands; the LymphChip project with project number NWA- ORC 2019 1292.19.019 of the NWA research program 'Research on Routes by Consortia (ORC)', which is funded by the Netherlands Organization for Scientific Research (NWO); The Novo Nordisk Foundation Center for Stem Cell Medicine is supported by Novo Nordisk Foundation grants (NNF21CC0073729).

Author Contirubutions

Conceptualization, V.V.O.; methodology, U.A., and V.V.O.; software, U.A., D.N., J.S., and B.v.M.; validation, U.A., M.B., V.M; formal analysis, U.A.; investigation, U.A., M.B., V.M, D.M.N., R.W.J.v.H, J.M.S., F.E.v.d.H.,B.v.M, M.V.C; visualisation, U.A.; resources, C.L.M. and V.V.O.; writing – original draft, U.A., M.B., C.L.M., and V.V.O.; writing – review & editing, U.A., C.L.M., and V.V.O.; supervision, C.L.M., and V.V.O.; project administration, V.V.O.; funding acquisition, C.L.M., and V.V.O.

Declaration Of Interest

C.L.M. is a cofounder of Pluriomics B.V. (now Ncardia B.V.).

References

Abe, Y., Watanabe, M., Chung, S., Kamm, R.D., Tanishita, K., and Sudo, R. (2019). *Balance of interstitial flow magnitude and vascular endothelial growth factor concentration modulates three-dimensional microvascular network formation.* APL Bioeng. 3, 36102. https://doi.org/10.1063/1.5094735.

Amersfoort, J., Eelen, G., and Carmeliet, P. (2022). *Immunomodulation by endothelial cells — partnering up with the immune system?* Nat. Rev. Immunol. 22, 576–588. https:// doi.org/10.1038/s41577-022-00694-4.

Arslan, U., Moruzzi, A., Nowacka, J., Mummery, C.L., Eckardt, D., Loskill, P., and Orlova, V. V. (2022). *Microphysiological stem cell models of the human heart.* Mater. Today Bio 14. https://doi.org/10.1016/j.mtbio.2022.100259.

Berg, C.W. van den, Elliott, D.A., Braam, S.R., Mummery, C.L., and Davis, R.P. (2016). *Differentiation of Human Pluripotent Stem Cells to Cardiomyocytes Under Defined Conditions.* Methods Mol. Biol. 1353, 163–180. https://doi.org/10.1007/7651_2014_178.

Berry, C., and Duncker, D.J. (2020). *Coronary microvascular disease: The next frontier for Cardiovascular Research.* Cardiovasc. Res. 116. https://doi.org/10.1093/cvr/cvaa035.

Carpenter, A.E., Jones, T.R., Lamprecht, M.R., Clarke, C., Kang, I.H., Friman, O., Guertin, D.A., Chang, J.H., Lindquist, R.A., Moffat, J., et al. (2006). *CellProfiler: image analysis software for identifying and quantifying cell phenotypes.* Genome Biol. 7, R100. https://doi.org/10.1186/gb-2006-7-10-r100.

Galie, P.A., Nguyen, D.H.T., Choi, C.K., Cohen, D.M., Janmey, P.A., and Chen, C.S. (2014). *Fluid shear stress threshold regulates angiogenic sprouting.* Proc. Natl. Acad. Sci. U. S. A. 111, 7968–7973. https://doi.org/10.1073/pnas.1310842111.

Giacomelli, E., Bellin, M., Orlova, V. V, and Mummery, C.L. (2017). *Co-Differentiation of Human Pluripotent Stem Cells-Derived Cardiomyocytes and Endothelial Cells from Cardiac Mesoderm Provides a Three-Dimensional Model of Cardiac Microtissue.* Curr. Protoc. Hum. Genet. 95, 21.9.1-21.9.22. https://doi.org/10.1002/cphg.46.

Giacomelli, E., Meraviglia, V., Campostrini, G., Cochrane, A., Cao, X., van Helden, R.W.J., Krotenberg Garcia, A., Mircea, M., Kostidis, S., Davis, R.P., et al. (2020). *Human-iPSC-Derived Cardiac Stromal Cells Enhance Maturation in 3D Cardiac Microtissues and Reveal Non-cardiomyocyte Contributions to Heart Disease.* Cell Stem Cell 26, 862-879.e11. https://doi.org/10.1016/j.stem.2020.05.004.

Guadix, J.A., Orlova, V. V, Giacomelli, E., Bellin, M., Ribeiro, M.C., Mummery, C.L., Pérez-Pomares, J.M., and Passier, R. (2017). *Human Pluripotent Stem Cell Differentiation into Functional Epicardial Progenitor Cells.* STEMCR 9, 1754–1764. https://doi.org/10.1016/j.stemcr.2017.10.023.

Hotaling, N.A., Bharti, K., Kriel, H., and Simon, C.G. (2015). *DiameterJ: A validated open source nanofiber diameter measurement tool.* Biomaterials 61. https://doi.org/10.1016/j.biomaterials.2015.05.015.

Mansour, A.A., Gonçalves, J.T., Bloyd, C.W., Li, H., Fernandes, S., Quang, D., Johnston, S., Parylak, S.L., Jin, X., and Gage, F.H. (2018). *An in vivo model of functional and vascularized human brain organoids.* Nat. Biotechnol. 36. https://doi.org/10.1038/nbt.4127.

Niccoli, G., Scalone, G., Lerman, A., and Crea, F. (2016). *Coronary microvascular obstruction in acute myocardial infarction.* Eur. Heart J. 37. https://doi.org/10.1093/eurheartj/ehv484.

Orlova, V. V., Van Den Hil, F.E., Petrus-Reurer, S., Drabsch, Y., Ten Dijke, P., and Mummery, C.L. (2014). *Generation, expansion and functional analysis of endothelial cells and pericytes derived from human pluripotent stem cells.* Nat. Protoc. https://doi.org/10.1038/nprot.2014.102.

Rostovskaya, M., Fu, J., Obst, M., Baer, I., Weidlich, S., Wang, H., Smith, A.J.H., Anastassiadis, K., and Francis Stewart, A. (2012). *Transposon-mediated BAC transgenesis in human ES cells. Nucleic Acids* Res. 40. https://doi.org/10.1093/nar/gks643.

Ryan, A.R., England, A.R., Chaney, C.P., Cowdin, M.A., Hiltabidle, M., Daniel, E., Gupta, A.K., Oxburgh, L., Carroll, T.J., and Cleaver, O. (2021). *Vascular deficiencies in renal organoids and ex vivo kidney organogenesis.* Dev. Biol. 477. https://doi.org/10.1016/j.ydbio.2021.04.009.

Takebe, T., Sekine, K., Enomura, M., Koike, H., Kimura, M., Ogaeri, T., Zhang, R.R., Ueno, Y., Zheng, Y.W., Koike, N., et al. (2013). *Vascularized and functional human liver from an iPSC-derived organ bud transplant.* Nature 499. https://doi.org/10.1038/nature12271.

Vila Cuenca, M., Cochrane, A., van den Hil, F.E., de Vries, A.A.F., Lesnik Oberstein, S.A.J., Mummery, C.L., and Orlova, V. V. (2021). *Engineered 3D vessel-on-chip using hiPSC-derived endothelial- and vascular smooth muscle cells.* Stem Cell Reports 16. https://doi.org/10.1016/j.stemcr.2021.08.003.

Zhang, M., D'Aniello, C., Verkerk, A.O., Wrobel, E., Frank, S., Ward-Van Oostwaard, D., Piccini, I., Freund, C., Rao, J., Seebohm, G., et al. (2014). *Recessive cardiac phenotypes in induced pluripotent stem cell models of Jervell and Lange-Nielsen syndrome: Disease mechanisms and pharmacological rescue.* Proc. Natl. Acad. Sci. U. S. A. 111. https://doi.org/10.1073/pnas.1419553111.

Zhang, S., Wan, Z., and Kamm, R.D. (2021). *Vascularized organoids on a chip: strategies for engineering organoids with functional vasculature.* Lab Chip 21, 473–488. https://doi.org/10.1039/d0lc01186j.

Zhang, S., Wan, Z., Pavlou, G., Zhong, A.X., Xu, L., Kamm, R.D., Zhang, S., Wan, Z., Pavlou, G., Zhong, A.X., et al. (2022). *Interstitial Flow Promotes the Formation of Functional Microvascular Networks In Vitro through Upregulation of Matrix Metalloproteinase-2.* Adv. Fun https://doi.org/10.1002/adfm.202206767.